Absolute triple differential cross sections for low-energy electron impact ionization of biochemically relevant systems: Water, tetrahydrofuran, and hydrated tetrahydrofuran

Jiaqi Zhou[1,2] Esam Ali[3,4] Maomao Gong,[5,6] Shaokui Jia,[1] Yutian Li,[1] Yingying Wang,[1] Zhen Zhang[1] Xiaorui Xue,[1]
Dmitry V. Fursa,[7] Igor Bray[7] Xiangjun Chen,[5,6] Don Madison,[8] Alexander Dorn,[2] and Xueguang Ren[1,2,*]

[1]*School of Physics, Xi'an Jiaotong University, Xi'an 710049, China*
[2]*Max-Planck-Institut für Kernphysik, Saupfercheckweg 1, 69117 Heidelberg, Germany*
[3]*Department of Natural Sciences, D. L. Hubbard Center for Innovation, Northwest Missouri State University, Maryville, Missouri 64468, USA*
[4]*Department of Physics, Faculty of Arts & Sciences-El Marj, University of Benghazi, El Marj, Libya*
[5]*Hefei National Laboratory for Physical Sciences at Microscale and Department of Modern Physics,*
University of Science and Technology of China, Hefei, Anhui 230026, China
[6]*Synergetic Innovation Center of Quantum Information and Quantum Physics,*
University of Science and Technology of China, Hefei, Anhui 230026, China
[7]*Curtin Institute for Computation and Department of Physics and Astronomy, Curtin University, GPO Box U1987, Perth, WA 6845, Australia*
[8]*Department of Physics, Missouri University of Science and Technology, Rolla, Missouri 65409, USA*

An experimental procedure is reported, which provides the absolute triple differential cross sections (ATDCSs) for electron-impact ionization of large (bio)molecules. This type of measurements represents the most stringent tests for new or existing theoretical models. We will use this procedure to test the accuracy of the best currently available theoretical models for the problems of electron-impact (65 eV) ionization of the molecules water (H_2O), tetrahydrofuran (C_4H_8O), and their hydrogen-bonded dimer $H_2O \cdot C_4H_8O$. The cross sections were calculated using the molecular three-body distorted-wave (M3DW) model, the multicenter three-distorted-wave (MCTDW) approach, and the multicenter three-distorted-wave using the Ward-Macek approximation (MCTDW-WM). When compared to the new experimental ATDCS results which cover almost the full solid angle of the ejected electron and a broad range of ejected electron energies and projectile scattering angles, it is found that the data for water are generally well reproduced by the M3DW model, while strong deviations in the absolute magnitude of the cross sections are found for the MCTDW. The MCTDW-WM model provides improved agreement over the MCTDW. These theoretical models, however, become less adequate for the ATDCS of C_4H_8O, in particular concerning the absolute magnitude. Furthermore, we find that a water environment can play a noticeable role for the ionization dynamics in the case of hydrated molecules.

I. INTRODUCTION

One of the primary goals of basic research is to determine and understand the strength and importance of interactions between fundamental particles. Since the universe is primarily composed of atoms, molecules, and charged particles, understanding charged particle interactions between atoms and molecules has been of primary interest since the beginning of quantum mechanics.

The electron-impact ionization problem is particularly challenging due to resulting in three, or more, charged particles which continue to interact at large distances via the long-ranged Coulomb potential. Even the proper formulation of the corresponding scattering amplitudes remained an intractable problem until the surface-integral approach to scattering theory given by [1]. Despite this, considerable progress has been made with sophisticated computational approaches to the problem in the case of simple atomic targets such as hydrogen and He [2–9]. The reason for the success of these approaches was then analyzed and understood [10].

The above-mentioned approaches all require a very accurate description of the target atom, and hence are restricted to quasi one- and two-electron targets. This is not possible in the case of multielectron molecules considered here. For large (bio)molecules, the only currently available theoretical models are based upon perturbation theory (see, e.g., [11–22]).

Advancement of theoretical models requires reliable experimental data for comparison. The most detailed experimental measurements for charged particle ionization of targets have been labeled triple differential cross sections (TDCS) and these types of measurements were pioneered by Ehrhardt *et al.* [23] and Amaldi *et al.* [24] and subsequent works in many groups for electron-atom scattering (see, e.g., [25,26]). In

*renxueguang@xjtu.edu.cn

the TDCS measurement, the energy of the incident charged particle is determined, the target state of the ionized target electron is determined, and the energies and angular locations of both final state continuum charged particles are determined. In other words, everything about the interaction is determined except the spins of the involved particles.

The initial TDCS measurements for atoms and molecules were able to get results for ionization of a particular target state. These measurements contained no information about the absolute values of the cross sections so only shape comparisons with theory could be used to evaluate the accuracy of theory. Multiple measurements for ionization of different states of the same target provided multiple shape comparisons which provided additional insight into the validity of theory but it was possible that a theory could provide reasonable shapes but entirely incorrect absolute magnitudes.

The next experimental advancement was the advent of cross-normalized TDCS measurements for which the absolute magnitude of all the measured individual cross sections were determined relative to the cross section of one of the target states which was not determined [27,28]. Again, this provided additional insight into the validity of the theoretical calculations but it was still possible that a theory could get the relative cross sections correct [20–22] and the absolute magnitude totally wrong.

The most severe test of theory would be to have experimental measurements which determined the absolute value of all the measured cross sections, and here we report this type of absolute TDCS (ATDCS) measurement for electron-biomolecules scattering. Currently, the best available theoretical models for calculating the TDCS for larger biomolecules are based upon perturbation theory so we will compare with the results of these models. However, it is anticipated that the present results will stimulate the development of improved models which can be tested for different targets and kinematics using the present procedure for measuring the ATDCS. Consequently, the experimental procedure presented here will provide the most stringent test for any theoretical advancement in this field.

The specific problems we have chosen for our first experimental ATDCS measurements are electron impact ionization of water (H_2O), tetrahydrofuran (THF, C_4H_8O), and hydrated THF particularly since these molecules have been previously studied for the case of nonabsolute measurements. Furthermore, we provide a study for the ionization of a weakly bound complex, i.e., the $H_2O \cdot C_4H_8O$ dimers. Here, H_2O and the deoxyribose-analog THF are considered as prototypes for modeling radiation-induced processes in biological systems [29–35]. The comparison of data for THF, H_2O, and $H_2O \cdot C_4H_8O$ dimers provides insight into the influence of the aqueous environment on biomolecules and whether or not the TDCS obtained for the gas phase can be directly used to model electron propagation in such media.

The absolute scale of the TDCS is obtained using He as a reference gas [36–38], whose absolute cross sections can be calculated reliably [10,25]. We use projectile electrons with 65 eV energy, which is close to the mean energy of secondary electrons produced by primary ionizing radiation [39]. The ATDCS measurements reported here cover a range of ejected energies (5–15 eV) and scattering angles ($-10°$–$-20°$).
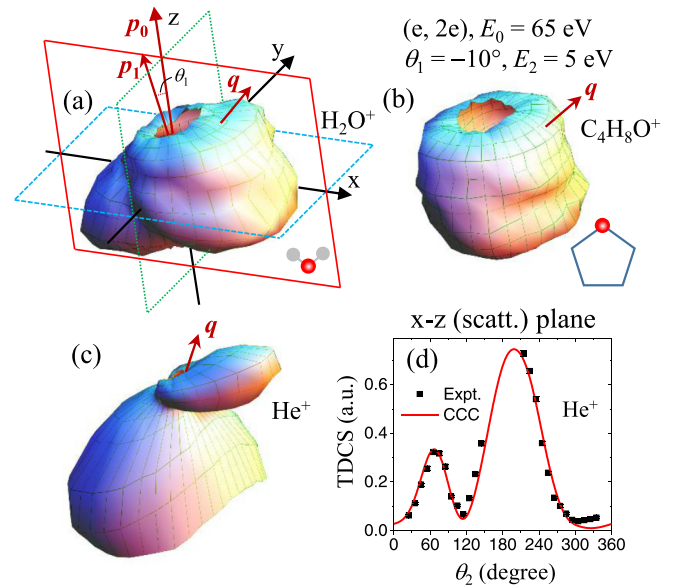

FIG. 1. (a)–(c) Measured TDCS presented as 3D images for the ionization of H_2O ($1b_1 + 3a_1$), THF ($0.8 \times 9b + 0.2 \times 12a'$), and He($1s$), respectively. The scattering angle is $\theta_1 = -10°$, and the ejected electron energy is $E_2 = 5$ eV. (d) Experimental (solid square) and CCC (red line) calculated TDCS for He in the x-z (scattering) plane.

II. EXPERIMENTAL METHOD

Experiments were carried out using a multiparticle momentum imaging spectrometer (reaction microscope) combined with a photoemission electron source and a heatable gas jet. This technique was described in detail elsewhere (see, e.g., [40,41]), so only a brief outline will be given here. The electron beam is crossed with a supersonic gas jet, which was generated in an expansion of He gas (1 bar) seeded with mixed water and THF vapor [42]. The projectile electrons with an energy width of about 0.5 eV are produced by photoemission from a tantalum cathode using UV-light pulses of 0.5 ns duration [43]. Homogeneous magnetic (7 G) and electric (1 V/cm) fields guide electrons and ions from the reaction volume onto two position- and time-sensitive detectors.

The data are recorded by triple coincidence detection of two electrons and the recoil ion. The three-dimensional (3D) momentum vectors of the final-state electrons and ions are determined from the measured times of flight and positions. The detection solid angle for He$^+$, H_2O^+, and THF$^+$ ions is 4π. The acceptance angle for detection of electrons up to an energy of 15 eV is also close to 4π, except for the acceptance holes at small forward and backward angles where the electrons end up in the detector bore. Since the complete experimentally accessible phase space is measured simultaneously in full 3D TDCS [see Figs. 1(a)–1(c)], all relative data for one target species are cross-normalized and a single global factor is required to place the measured TDCS onto an absolute scale.

III. ABSOLUTE CALIBRATION PROCEDURE

In the following, the method used for absolute calibration of the measured TDCS is described. Thereby, we circumvent
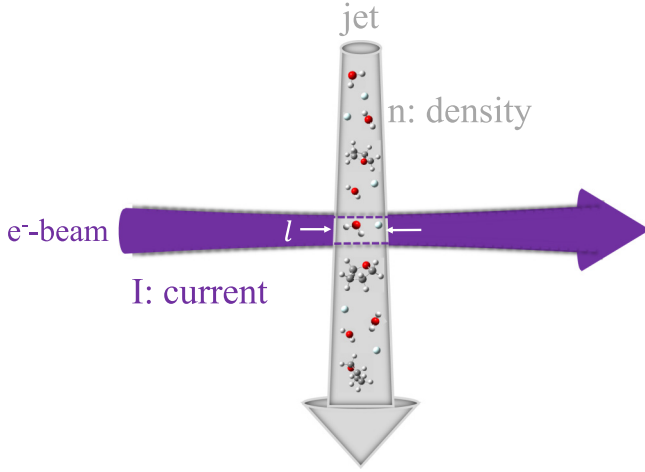
FIG. 2. Illustration for determining the absolute cross section of the crossed-beam reaction.

the cumbersome determination of the absolute target densities and the ion detection efficiencies. Therefore, published data for the absolute total ionization cross sections for all targets and for the ATDCS of He are used. Additionally, the measurements were done on a target jet containing a mixture of all species studied, such that the experimental conditions were identical.

Experimentally, all detected electrons are accelerated to about 200 eV plus their initial kinetic energy before hitting on the microchannel plates of the detector. Therefore, the differences of the impact energies and the resulting detection efficiencies for both the scattered and ejected electrons are relatively small. The ionization cross sections of He, the two outermost orbitals $1b_1$ and $3a_1$ of H_2O, and the highest occupied molecular orbital (HOMO) of THF as well as of the hydrogen-bonded dimer $H_2O \cdot C_4H_8O$ were measured simultaneously, leading to He^+, H_2O^+ [20], $C_4H_8O^+$ [43], and $H_2O \cdot C_2H_4O^+$ [35] cations, respectively. Taking H_2O^+ as an example, we measured directly the triple coincidence rate $\dot{N}_{H_2O^+}^{TDCS}$ corresponding to the relative TDCS and the total ion yield $\dot{N}_{H_2O^+}^T$ corresponding to the total ionization cross section for producing this ion (total partial ionization cross section).

The relative target densities of He, H_2O, and C_4H_8O in the gas jet are related to the measured ion yields and the total ionization cross sections of $\sigma_{He^+}^T$ [44], $\sigma_{H_2O^+}^T$ [45], and $\sigma_{C_4H_8O^+}^T$ [46,47]. The measured ion yield, e.g., $\dot{N}_{H_2O^+}^T$, can be described as

$$\dot{N}_{H_2O^+}^T = n_{H_2O} I \sigma_{H_2O^+}^T l \epsilon_{H_2O^+}. \tag{1}$$

Here n_{H_2O}, I, $\sigma_{H_2O^+}^T$, l, and $\epsilon_{H_2O^+}$ represent the water molecule density, the electron beam current, the total partial ionization cross section, the reaction volume length, and the detection efficiency for H_2O^+ ions, respectively (see Fig. 2). Thus, the water molecule density n_{H_2O} is

$$n_{H_2O} = \frac{\dot{N}_{H_2O^+}^T}{I \sigma_{H_2O^+}^T l \epsilon_{H_2O^+}}. \tag{2}$$

Since I and l are identical for all target species, the density ratio between H_2O and He in the gas jet can be written as

$$\frac{n_{H_2O}}{n_{He}} = \frac{\dot{N}_{H_2O^+}^T \sigma_{He^+}^T \epsilon_{He^+}}{\dot{N}_{He^+}^T \sigma_{H_2O^+}^T \epsilon_{H_2O^+}}. \tag{3}$$

In the following, we determine the ATDCS from the relative measurements, e.g., $\dot{N}_{H_2O^+}^{TDCS}$, which can be described as

$$\sigma_{H_2O^+}^{TDCS} = \frac{\dot{N}_{H_2O^+}^{TDCS}}{n_{H_2O} I l \epsilon_{H_2O^+}}, \tag{4}$$

where $\sigma_{H_2O^+}^{TDCS}$ is the ATDCS of water molecule for H_2O^+ product. Therefore, the TDCS ratio between H_2O^+ and He^+ can be determined as

$$\frac{\sigma_{H_2O^+}^{TDCS}}{\sigma_{He^+}^{TDCS}} = \frac{\dot{N}_{H_2O^+}^{TDCS} n_{He} \epsilon_{He^+}}{\dot{N}_{He^+}^{TDCS} n_{H_2O} \epsilon_{H_2O^+}}. \tag{5}$$

By substituting Eq. (3) into the above formula, we further obtain the TDCS ratio as

$$\begin{aligned}\frac{\sigma_{H_2O^+}^{TDCS}}{\sigma_{He^+}^{TDCS}} &= \frac{\dot{N}_{H_2O^+}^{TDCS} \dot{N}_{He^+}^T \sigma_{H_2O^+}^T \epsilon_{H_2O^+} \epsilon_{He^+}}{\dot{N}_{He^+}^{TDCS} \dot{N}_{H_2O^+}^T \sigma_{He^+}^T \epsilon_{He^+} \epsilon_{H_2O^+}} \\ &= \frac{\dot{N}_{H_2O^+}^{TDCS} \dot{N}_{He^+}^T \sigma_{H_2O^+}^T}{\dot{N}_{He^+}^{TDCS} \dot{N}_{H_2O^+}^T \sigma_{He^+}^T}. \end{aligned} \tag{6}$$

Importantly, the detection efficiencies drop out. The ATDCS for He^+ ($\sigma_{He^+}^{TDCS}$) can be obtained reliably using the theoretical convergent close coupling (CCC) mehtod or taken from published experiments [10,25]. As a result, the ATDCS for water molecule $\sigma_{H_2O^+}^{TDCS}$ can be determined as

$$\sigma_{H_2O^+}^{TDCS} = \dot{N}_{H_2O^+}^{TDCS} \frac{\sigma_{He^+}^{TDCS}}{\dot{N}_{He^+}^{TDCS}} \frac{\dot{N}_{He^+}^T}{\dot{N}_{H_2O^+}^T} \frac{\sigma_{H_2O^+}^T}{\sigma_{He^+}^T}. \tag{7}$$

Therefore, a general formula is obtained for determining the ATDCS of a system (X) if He data are obtained simultaneously:

$$\sigma_{X^+}^{TDCS} = \dot{N}_{X^+}^{TDCS} \frac{\sigma_{He^+}^{TDCS}}{\dot{N}_{He^+}^{TDCS}} \cdot \frac{\dot{N}_{He^+}^T}{\dot{N}_{X^+}^T} \frac{\sigma_{X^+}^T}{\sigma_{He^+}^T}, \tag{8}$$

where X^+ can be replaced by $C_4H_8O^+$, $H_2O \cdot C_2H_4O^+$, and so on. For THF, a small part of the HOMO ionization can cause the dissociation of $C_4H_8O^+$ into $C_4H_7O^+$ and H [43], the measured cross sections for $C_4H_8O^+$ were therefore multiplied by a factor of $1/(1 - r)$ with r being the dissociation rate (20%) to determine the ATDCS for the HOMO ionization. As mentioned above, the ion detection efficiencies cancel out in the present method to calibrate the absolute scale. This means that the method can also be applied to obtain the absolute cross sections for specific ionization channels in which the ionic species might not be fully detected, such as molecular dissociation processes. It is also to be noted that this method can be used to determine the absolute double differential cross sections of different atoms and molecules.

Concerning the measurement of the $H_2O \cdot C_4H_8O$ dimer, there are no literature data for the absolute ionization cross section of $H_2O \cdot C_4H_8O$. Therefore, we use the $\sigma_{C_4H_8O^+}^T$ [46,47] to calibrate the ATDCS of HOMO ionization of

$H_2O \cdot C_4H_8O$, which leads to $H_2O \cdot C_2H_4O^+$ cation [35]. This means that we assume $\sigma^T_{H_2O \cdot C_2H_4O^+} \approx \sigma^T_{C_4H_8O^+}$ as both channels are initiated by HOMO ionization of THF.

The global scaling factor is obtained by scaling the measured TDCS of He$^+$ with the CCC calculation, in which an excellent agreement is achieved concerning the TDCS pattern [see the results for $\theta_1 = -10°$ and $E_2 = 5$ eV in Fig. 1(d)]. The uncertainty in the measured cross sections is 10%, which is mainly caused by the ion yield deviations during the measurements.

IV. THEORETICAL MODELS

We compare the experimental results with the two best currently available theoretical models, i.e. the molecular three-body distorted-wave approach (M3DW) and the multi-center three-distorted-wave approach (MCTDW). The details of the theoretical approaches have already been discussed in [11,18] for M3DW and [22] for MCTDW. In general, all calculations describe the three continuum electrons by a distorted wave. The M3DW model contains the final-state Coulomb-distortion factor between the two electrons, normally called the post-collision interaction (PCI) exactly, while no PCI is included in MCTDW. We have also carried out MCTDW-WM calculations where the PCI effect is approximated by the Gamow factor calculated with the Ward-Macek (WM) method [48]. More detailed information can be found in the references given.

V. RESULTS AND DISCUSSIONS

The experimental resolution (2.0 eV) of the sum energy of both outgoing electrons is not sufficient to uniquely identify the ionized molecular orbital. On the other hand, the coincident detection of the residual ion provides a restriction on the number of contributing orbitals. Here only the production of intact H_2O^+ and $C_4H_8O^+$ cations are considered. Therefore, the data for H_2O^+ represent the summed ATDCS for the ionization of the two highest orbitals $1b_1$ and $3a_1$ [20]. For THF, ionization of the HOMO produces $C_4H_8O^+$. Thus, the $C_4H_8O^+$ data represent the ATDCS for the ionization of $9b$ (80%) and $12a'$ (20%) orbitals for the C_2 and C_s conformers of THF [49], respectively.

The experimental TDCS as 3D polar plots for H_2O, C_4H_8O, and He are presented in Figs. 1(a)–1(c), respectively, for a projectile scattering angle of $\theta_1 = -10°$ as a function of the emission direction of a slow ejected electron with $E_2 = 5$ eV energy. In these 3D plots, the projectile (p_0) enters from the bottom and is scattered to the left (p_1). These two vectors define the scattering (x-z) plane, as marked by the solid red frame in panel (a). The momentum transfer to the target is indicated by the arrow labeled q. The TDCS for a particular direction is given as the distance from the origin of the plot to the point on the surface, which is intersected by the ejected electron's emission direction.

In Fig. 1(c), the TDCS of He is governed by the well-known binary and recoil lobes [8]. The binary lobe is oriented roughly along the q direction, corresponding to electrons emitted after a single binary collision with the projectile. In the opposite direction the recoil lobe is found, where

the outgoing electron, initially moving in the q direction, backscatters in the ionic potential. Both lobes are shifted backwards since the emitted electron is repelled by the scattered projectile due to the strong PCI effect at the present low-impact energy. For the H_2O target in Fig. 1(a), both lobes can also be identified. However, the shape and the relative size of these two lobes are significantly changed. This is even more pronounced for the TDCS of C_4H_8O, where the two lobes tend to merge or are partially superimposed on one another, as shown in Fig. 1(b).

In the following, we compare the ATDCS with the results from the M3DW and MCTDW models. Cuts through the 3D TDCS patterns along the three orthogonal planes as indicated in Fig. 1(a) are presented in Figs. 3 and 4 for the results of H_2O and C_4H_8O, respectively. Those are the x-z (scattering) plane [solid frame Fig. 1(a)], the y-z (perpendicular) plane (dotted frame), and the x-y (full-perpendicular) plane (dashed frame). In Figs. 3 and 4, these planes are shown in the left, middle, and right columns of the figures, respectively.

The patterns in Fig. 3 are generally in line with the previous $(e, 2e)$ studies of H_2O at 81 eV [20–22]. The observed features include the small minimum or dip near the q direction for the smaller ejected energy case $E_2 = 5$ eV, which is the result of the characteristic momentum profile of the p-type orbital ($1b_1$ and $3a_1$ for H_2O). Here, one smaller peak close to the projectile scattering (i.e., near-forward) direction and one larger peak at larger angles with respect to q are observed. The imbalance is caused by the PCI effect. In the perpendicular plane, there is an indication of a three-lobe structure with two symmetric maxima at θ_2 near 60° and 270° and one central maximum at $\theta_2 = 180°$ caused by the recoil lobe. In the full-perpendicular plane, which is perpendicular to the incident-projectile direction, the ejected electron's polar angle is fixed at $\theta_2 = 90°$ and the azimuthal angle ϕ_2 is varied. The observed structures for emission at ϕ_2 near 0° and also for some cases near 30° and 330° are caused by the binary peak. The recoil peak most likely influences the cross sections near $\phi_2 = 180°$. In this plane the influence of PCI is comparatively small over the entire angular range.

The present ATDCSs are generally well reproduced by M3DW calculations, while we observe strong deviations between MCTDW and experiment, in particular for small mutual angles of the outgoing electrons and for the absolute magnitude of the cross sections. The MCTDW-WM with the inclusion of PCI effect shows much better agreement with the experimental data, regarding the angular dependence of the TDCS. It is noted that the calculations were multiplied by factors of 0.5 and 1.8 for the MCTDW and MCTDW-WM models, respectively. In the full-perpendicular plane, good agreement is also found for MCTDW because of the smaller influence of PCI in this plane. In addition, the M3DW tends to predict higher recoil lobes, as seen in the peaks at $\theta_2 \sim 200°$ in the scattering plane and for some cases $\phi_2 = 180°$ in the full-perpendicular plane. A noticeable systematic difference occurs in the perpendicular plane, where the two symmetric maxima at $\theta_2 \sim 60°$ and 300° are not indicated in the calculations, in particular for the smaller ejected energies of $E_2 = 5$ and 10 eV.

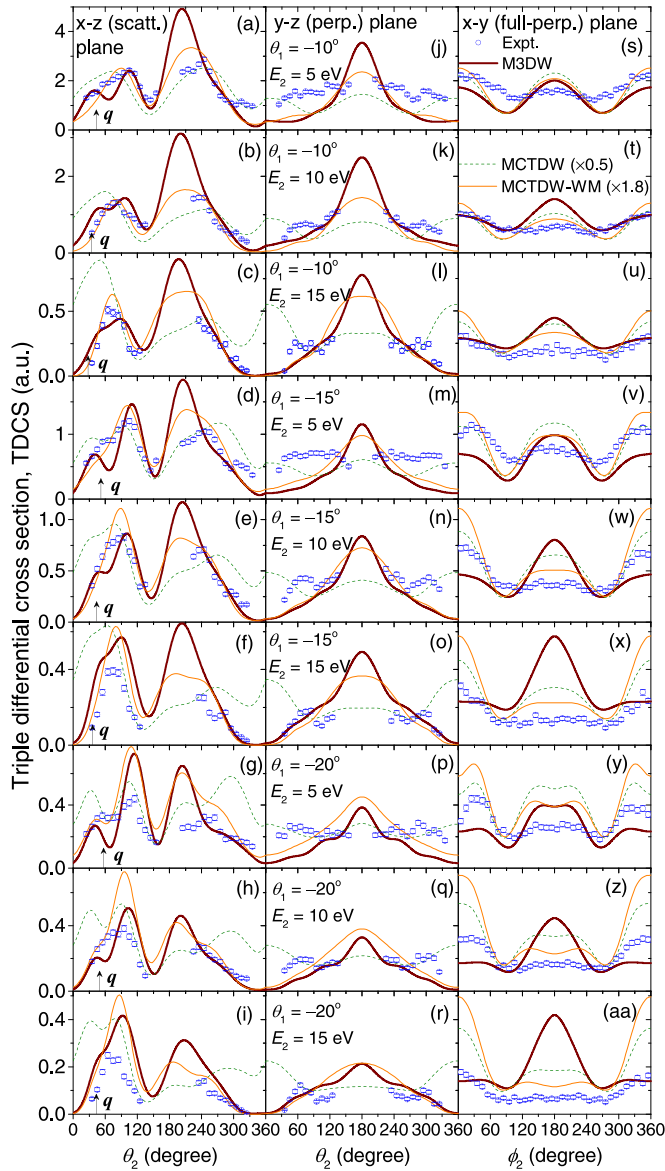Figure 4 shows a comparison between experiment and theories for the ATDCS of C_4H_8O in the three planes. Overall,

FIG. 3. ATDCS for the ionization of H_2O ($1b_1 + 3a_1$) as a function of the ejected electron emission angle for different scattering angles θ_1 ($-10° \pm 3°$, $-15° \pm 4°$, and $-20° \pm 4°$) and ejected electron energies E_2 (5 ± 2.5 eV, 10 ± 3 eV, and 15 ± 4 eV). Left column: TDCS in the x-z (scattering) plane. Middle column: TDCS in the y-z (perpendicular) plane. Right column: TDCS in the x-y (full-perpendicular) plane. The various kinematics (θ_1, E_2) are labeled in the panels of the middle column. The open circles with error bars represent the experimental data. Thick solid lines: M3DW; thin solid lines: MCTDW-WM; thin dashed lines: MCTDW model.

FIG. 4. Same as Fig. 3 but for the ionization of THF ($0.8 \times 9b + 0.2 \times 12a'$), leading to the intact $C_4H_8O^+$ cation.

the agreement between experiment and theories is not as good as it is for H_2O not only in the angular dependence of the cross sections but also in the absolute magnitude. Here, in order to compare properly with the experimental data, the calculations were multiplied by factors of 0.75, 2.5, and 6.25 for M3DW, MCTDW, and MCTDW-WM models, respectively.

Regarding the angular dependence, the present TDCS show similar tendencies in comparison with the previous study at 91 eV [49], particularly for the full-perpendicular
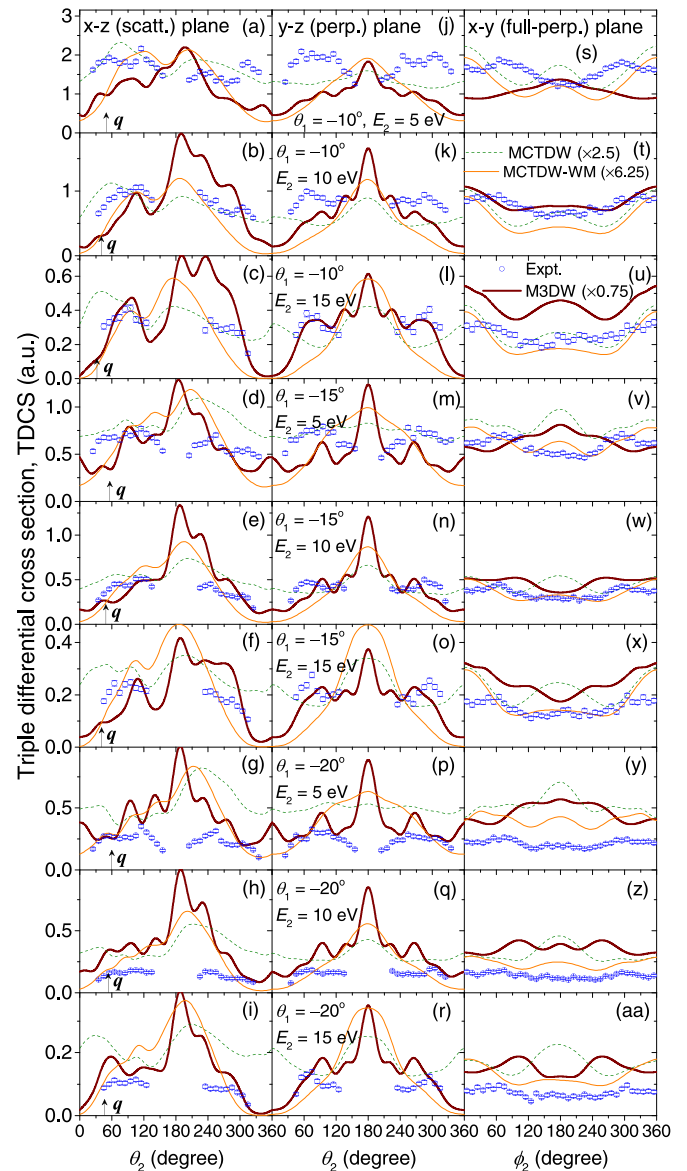
plane. Additionally, we see changes on the peak height and position of the binary and recoil patterns between these two experiments. Here, the binary lobes are better reproduced by the M3DW and MCTDW-WM calculations compared to MCTDW, in particular for the higher ejected energies. This is consistent with the effect of PCI which is accounted for by M3DW and MCTDW-WM. Higher recoil lobes than shown by experiment and MCTDW-WM are often predicted by M3DW, in particular for the results in Figs. 4(b) and 4(c). In the perpendicular plane, two maxima are clearly visible at θ_2 near 60° and 300°, which are well reproduced by the M3DW for the higher ejected energy of 15 eV. In the full-perpendicular plane, the binary pattern contains two maxima at ϕ_2 near 60° and 300° and also for some cases a broad maximum at ϕ_2 near 0°. We can see a flat distribution or minimum at ϕ_2 near 180° for the recoil patterns. These features are also generally reproduced by both the M3DW and MCTDW-WM
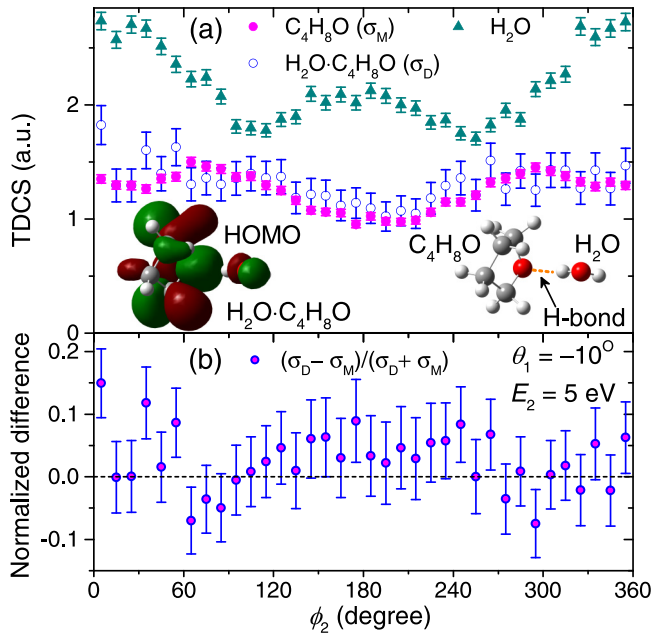
FIG. 5. (a) Measured ATDCS in the full-perpendicular plane for HOMO ionization of the $H_2O \cdot C_4H_8O$ dimer (open circles) and C_4H_8O (solid circles). Full triangles are ATDCS for water which is shifted upwards by 0.5 a.u. The insets show the molecular structure of $H_2O \cdot C_4H_8O$ and its HOMO orbital. (b) The normalized difference between the TDCS of $H_2O \cdot C_4H_8O$ dimer (σ_D) and C_4H_8O monomer (σ_M).

calculations, especially for $E_2 = 10$ and 15 eV. While for MCTDW, a maximum at $\phi_2 = 180°$ is predicted for all the cases.

Finally, we present measurements for the HOMO ionization of the hydrogen-bonded $H_2O \cdot C_4H_8O$ dimer which is equivalent to the removal of an electron from the outermost orbital of the C_4H_8O. As discussed before by Wang *et al.* [35] this leads to a ring-break reaction and the formation of a $H_2O \cdot C_2H_4O^+$ cation. The measured ATDCS in the full-perpendicular plane is presented in Fig. 5 for $\theta_1 = -10°$ and $E_2 = 5$ eV. The result for C_4H_8O monomer is also included for comparison. As can be seen in Fig. 5(a), the ATDCS for $H_2O \cdot C_4H_8O$ is generally very similar to that obtained for the C_4H_8O molecule. On the other hand, the TDCS pattern for H_2O, which is shown in the same panel, is clearly different. This confirms that the $H_2O \cdot C_2H_4O^+$ product originates from ionization of the C_4H_8O HOMO in the dimers.

To get more insight into the dynamics of $H_2O \cdot C_4H_8O$, we show the normalized difference between the ATDCS of the $H_2O \cdot C_4H_8O$ dimer (σ_D) and the C_4H_8O monomer (σ_M), i.e., $(\sigma_D - \sigma_M)/(\sigma_D + \sigma_M)$. This difference, as shown in Fig. 5(b), is not zero but is positive at ϕ_2 around 0° and 180° and shows minima in the ranges $\phi_2 = 60°–90°$ and $270°–300°$. This indicates that the neighboring H_2O molecule influences the ionization dynamics of $H_2O \cdot C_4H_8O$. The HOMO of $H_2O \cdot C_4H_8O$, which is shown in the inset of Fig. 5(a), is mainly localized on the C_4H_8O site but it also includes a contribution from the H_2O. Therefore, one reason for the subtle differences in the TDCS patterns could be due to the differences of the ionized orbital wave functions. Another reason could be the

different multicenter potential in the final ionic state which is experienced by the ejected and the scattered electrons.

VI. CONCLUSION

In summary, we have reported an experimental procedure for obtaining ATDCSs. We have demonstrated the utility of this procedure by presenting a detailed study of the low-energy (65 eV) electron-impact ionization dynamics of water, THF (C_4H_8O), and the hydrated $H_2O \cdot C_4H_8O$ dimer. ATD-CSs have been obtained over a large part of the full solid angular range. The present results cover a range of projectile scattering angles θ_1 from $-10°$ to $-20°$ and ejected energies E_2 from 5 to 15 eV, thus providing a more rigorous testing ground for scattering theory. The present experimental method can be generally applied to various molecules to obtain ATDCSs. Here, the experimental ATDCSs for water are reasonably well reproduced by M3DW calculations, regarding both the angular dependence of the cross section and the absolute magnitude. In contrast, for the MCTDW strong deviations are seen in the absolute values of the cross sections and also in the angular dependence near the projectile forward direction due to the lack of PCI in this model. MCTDW-WM with inclusion of PCI provides significantly improved agreement with the shape of the experimental TDCS confirming the important role of PCI at low-impact energy.

The present calculations are less adequate for describing the ATDCS of THF not only for the angular dependence of the cross sections but also for the absolute magnitudes which differ strongly from each other and from experiment. Compared to experiment, the M3DW results were approximately a factor of 1.35 too large, while the MCTDW and MCTDW-WM results were a factor of 2.5 and 6.25 too small, respectively. Moreover, these methods were unable to provide reliable predictions for the $H_2O \cdot C_4H_8O$ dimer. The present results indicate that studying the ionization dynamics for larger systems like biomolecules or molecular complexes is still a challenging task which deserves more efforts, especially concerning the issue of absolute data. Furthermore, our study sheds light on the ionization dynamics of hydrated biomolecules in which the noticeable role of the water environment on the collision dynamics was demonstrated. This should be considered in future theoretical models. These results will enable progress in understanding radiation effects in aqueous environments including those related to energy production and waste processing, and in biology [29–32].

[1] A. S. Kadyrov, I. Bray, A. M. Mukhamedzhanov, and A. T. Stelbovics, Surface-integral formulation of scattering theory, Ann. Phys. **324**, 1516 (2009).

[2] I. Bray and D. V. Fursa, Calculation of ionization within the close-coupling formalism, Phys. Rev. A **54**, 2991 (1996).

[3] T. N. Rescigno, M. Baertschy, W. A. Isaacs, and C. W. McCurdy, Collisional breakup in a quantum system of three charged particles, Science **286**, 2474 (1999).

[4] M. Baertschy, T. N. Rescigno, and C. W. McCurdy, Accurate amplitudes for electron-impact ionization, Phys. Rev. A **64**, 022709 (2001).

[5] I. Bray, Close-Coupling Approach to Coulomb Three-Body Problems, Phys. Rev. Lett. **89**, 273201 (2002).

[6] J. Colgan, M. S. Pindzola, F. J. Robicheaux, D. C. Griffin, and M. Baertschy, Time-dependent close-coupling calculations of the triple-differential cross section for electron-impact ionization of hydrogen, Phys. Rev. A **65**, 042721 (2002).

[7] J. Röder, M. Baertschy, and I. Bray, Measurements of the ionization of atomic hydrogen by 17.6-eV electrons, Phys. Rev. A **67**, 010702(R) (2003).

[8] X. Ren, I. Bray, D. V. Fursa, J. Colgan, M. S. Pindzola, T. Pflüger, A. Senftleben, S. Xu, A. Dorn, and J. Ullrich, Electron-impact ionization of helium: A comprehensive experiment benchmarks theory, Phys. Rev. A **83**, 052711 (2011).

[9] O. Zatsarinny and K. Bartschat, Nonperturbative Treatment of Ionization with Excitation of Helium by Electron Impact, Phys. Rev. Lett. **107**, 023203 (2011).

[10] I. Bray, D. V. Fursa, A. S. Kadyrov, A. T. Stelbovics, A. S. Kheifets, and A. M. Mukhamedzhanov, Electron- and photon-impact atomic ionisation, Phys. Rep. **520**, 135 (2012).

[11] D. H. Madison and O. Al-Hagan, The distorted-wave born approach for calculating electron-impact ionization of molecules, J. At., Mol., Opt. Phys. **2010**, 367180 (2010).

[12] T. Khatir, S. Houamer, and C. Dal Cappello, Theoretical study of the collision dynamics in $(e, 2e)$ reactions, J. Phys. B: At., Mol. Opt. Phys. **52**, 245201 (2019).

[13] C. M. Granados-Castro and L. U. Ancarani, Electron impact ionization of the outer valence orbital $1t_2$ of CH_4, Eur. Phys. J. D **71**, 65 (2017).

[14] K. L. Nixon, A. J. Murray, O. Al-Hagan, D. H. Madison, and C. Ning, Low-energy symmetric coplanar and symmetric non-coplanar (e,2e) studies from the $3a_1$ state of H_2O, J. Phys. B: At., Mol. Opt. Phys. **43**, 035201 (2010).

[15] D. S. Milne-Brownlie, S. J. Cavanagh, B. Lohmann, C. Champion, P. A. Hervieux, and J. Hanssen, Dynamics in electron-impact ionization of H_2O, Phys. Rev. A **69**, 032701 (2004).

[16] C.-Y. Lin, C. W. McCurdy, and T. N. Rescigno, Complex Kohn approach to molecular ionization by high-energy electrons: Application to H_2O, Phys. Rev. A **89**, 012703 (2014).

[17] S. Zhang, X. Y. Li, J. G. Wang, Y. Z. Qu, and X. Chen, Multicenter distorted-wave method for fast-electron-impact single ionization of molecules, Phys. Rev. A **89**, 052711 (2014).

[18] E. Ali, H. S. Chakraborty, and D. H. Madison, Improved theoretical calculations for electron-impact ionization of DNA analogue molecules, J. Chem. Phys. **152**, 124303 (2020).

[19] D. Jones, J. Builth-Williams, S. Bellm, L. Chiari, H. Chaluvadi, D. Madison, C. Ning, B. Lohmann, O. Ingólfsson, and M. Brunger, Dynamical (e,2e) investigations of tetrahydrofuran and tetrahydrofurfuryl alcohol as DNA analogues, Chem. Phys. Lett. **572**, 32 (2013).

[20] X. Ren, S. Amami, K. Hossen, E. Ali, C. G. Ning, J. Colgan, D. Madison, and A. Dorn, Electron-impact ionization of H_2O at low projectile energy: Internormalized triple-differential cross sections in three-dimensional kinematics, Phys. Rev. A **95**, 022701 (2017).

[21] E. Acebal and S. Otranto, Continuum-distorted-wave eikonal-initial-state description of the electron-impact ionization of H_2O at low impact energies, Phys. Rev. A **98**, 012703 (2018).

[22] M. Gong, X. Li, S. B. Zhang, S. Niu, X. Ren, E. Wang, A. Dorn, and X. Chen, Multicenter three-distorted-wave approach to three-dimensional images for electron-impact-ionization dynamics of molecules: Overall agreement with experiment, Phys. Rev. A **98**, 042710 (2018).

[23] H. Ehrhardt, M. Schulz, T. Tekaat, and K. Willmann, Ionization of Helium: Angular Correlation of the Scattered and Ejected Electrons, Phys. Rev. Lett. **22**, 89 (1969).

[24] U. Amaldi, A. Egidi, R. Marconero, and G. Pizzella, Use of a two channeltron coincidence in a new line of research in atomic physics, Rev. Sci. Instrum. **40**, 1001 (1969).

[25] H. Ehrhardt, K. Jung, G. Knoth, and P. Schlemmer, Differential cross sections of direct single electron impact ionization, Z. Phys. D: At. Mol. Clusters **1**, 3 (1986).

[26] A. Lahmam-Bennani, Recent developments and new trends in (e,2e) and (e,3e) studies, J. Phys. B: At., Mol. Opt. Phys. **24**, 2401 (1991).

[27] T. Pflüger, O. Zatsarinny, K. Bartschat, A. Senftleben, X. Ren, J. Ullrich, and A. Dorn, Electron-Impact Ionization of Neon at Low Projectile Energy: An Internormalized Experiment and Theory for a Complex Target, Phys. Rev. Lett. **110**, 153202 (2013).

[28] X. Ren, S. Amami, O. Zatsarinny, T. Pflüger, M. Weyland, W. Y. Baek, H. Rabus, K. Bartschat, D. Madison, and A. Dorn, Kinematically complete study of low-energy electron-impact ionization of neon: Internormalized cross sections in three-dimensional kinematics, Phys. Rev. A **91**, 032707 (2015).

[29] M. J. Brunger, Electron scattering and transport in biofuels, biomolecules and biomass fragments, Int. Rev. Phys. Chem. **36**, 333 (2017).

[30] B. C. Garrett, D. A. Dixon, D. M. Camaioni, D. M. Chipman, M. A. Johnson, C. D. Jonah, G. A. Kimmel, J. H. Miller, T. N. Rescigno, P. J. Rossky *et al.*, Role of water in electron-initiated processes and radical chemistry: Issues and scientific advances, Chem. Rev. **105**, 355 (2005).

[31] K. Bartschat and M. J. Kushner, Electron collisions with atoms, ions, molecules, and surfaces: Fundamental science empowering advances in technology, Proc. Natl. Acad. Sci. USA **113**, 7026 (2016).

[32] E. Alizadeh, T. M. Orlando, and L. Sanche, Biomolecular damage induced by ionizing radiation: The direct and indirect effects of low-energy electrons on DNA, Annu. Rev. Phys. Chem. **66**, 379 (2015).

[33] A. G. Sanz, M. C. Fuss, A. Muñoz, F. Blanco, P. Limão-Vieira, M. J. Brunger, S. J. Buckman, and G. García, Modelling low energy electron and positron tracks for biomedical applications, Int. J. Radiat. Biol. **88**, 71 (2012).

[34] M. U. Bug, W. Yong Baek, H. Rabus, C. Villagrasa, S. Meylan, and A. B. Rosenfeld, An electron-impact cross section data

set (10 eV–1 keV) of DNA constituents based on consistent experimental data: A requisite for Monte Carlo simulations, Radiat. Phys. Chem. **130**, 459 (2017).

[35] E. Wang, X. Ren, W. Baek, H. Rabus, T. Pfeifer, and A. Dorn, Water acting as a catalyst for electron-driven molecular break-up of tetrahydrofuran, Nat. Commun. **11**, 2194 (2020).

[36] J. C. Nickel, P. W. Zetner, G. Shen, and S. Trajmar, Principles and procedures for determining absolute differential electron-molecule (atom) scattering cross sections, J. Phys. E **22**, 730 (1989).

[37] L. R. Hargreaves, M. A. Stevenson, and B. Lohmann, A simple method for absolute normalization of (e, 2e) cross sections, Meas. Sci. Technol. **21**, 055112 (2010).

[38] L. R. Hargreaves, M. A. Stevenson, and B. Lohmann, Absolute triple-differential cross sections for intermediate energy electron impact ionization of neon and argon, J. Phys. B: At., Mol. Opt. Phys. **43**, 205202 (2010).

[39] S. M. Pimblott and J. A. LaVerne, Production of low-energy electrons by ionizing radiation, Radiat. Phys. Chem. **76**, 1244 (2007).

[40] J. Ullrich, R. Moshammer, A. Dorn, R. Dörner, L. Schmidt, and H. Schmidt-Böcking, Recoil-ion and electron momentum spectroscopy: Reaction-microscopes, Rep. Prog. Phys. **66**, 1463 (2003).

[41] X. Ren, E. Jabbour Al Maalouf, A. Dorn, and S. Denifl, Direct evidence of two interatomic relaxation mechanisms in argon dimers ionized by electron impact, Nat. Commun. **7**, 11093 (2016).

[42] X. Ren, E. Wang, A. D. Skitnevskaya, A. B. Trofimov, K. Gokhberg, and A. Dorn, Experimental evidence for ultrafast intermolecular relaxation processes in hydrated biomolecules, Nat. Phys. **14**, 1062 (2018).

[43] X. Ren, T. Pflüger, M. Weyland, W. Y. Baek, H. Rabus, J. Ullrich, and A. Dorn, An (e, 2e + ion) study of low-energy electron-impact ionization and fragmentation of tetrahydrofuran with high mass and energy resolutions, J. Chem. Phys. **141**, 134314 (2014).

[44] R. Rejoub, B. G. Lindsay, and R. F. Stebbings, Determination of the absolute partial and total cross sections for electron-impact ionization of the rare gases, Phys. Rev. A **65**, 042713 (2002).

[45] Y. Itikawa and N. Mason, Cross sections for electron collisions with water molecules, J. Phys. Chem. Ref. Data **34**, 1 (2005).

[46] M. Fuss, A. Muñoz, J. C. Oller, F. Blanco, D. Almeida, P. Limão-Vieira, T. P. D. Do, M. J. Brunger, and G. García, Electron-scattering cross sections for collisions with tetrahydrofuran from 50 to 5000 eV, Phys. Rev. A **80**, 052709 (2009).

[47] M. Dampc, E. Szymańska, B. Mielewska, and M. Zubek, Ionization and ionic fragmentation of tetrahydrofuran molecules by electron collisions, J. Phys. B: At., Mol. Opt. Phys. **44**, 055206 (2011).

[48] S. J. Ward and J. H. Macek, Wave functions for continuum states of charged fragments, Phys. Rev. A **49**, 1049 (1994).

[49] E. Wang, X. Ren, M. Gong, E. Ali, Z. Wang, C. Ma, D. Madison, X. Chen, and A. Dorn, Triple-differential cross sections for (*e*, 2*e*) electron-impact ionization dynamics of tetrahydrofuran at low projectile energy, Phys. Rev. A **102**, 062813 (2020).